Probing the density of states in $EuFe_{2-x}Ru_xAs_2$

M. Hemmida,[1,2] H.-A. Krug von Nidda,[1] A. Günther,[1] A. Loidl,[1] A. Leithe-Jasper,[2] W. Schnelle,[2] H. Rosner,[2] and J. Sichelschmidt[2]

[1]*Experimental Physics V, Center for Electronic Correlations and Magnetism, Institute for Physics, University of Augsburg, 86135, Augsburg, Germany*

[2]*Max Planck Institute for Chemical Physics of Solids, 01187, Dresden, Germany*

(Received 1 August 2014; revised manuscript received 7 October 2014; published 4 November 2014)

The evolution of the electronic density of states at the Fermi level of intermetallic $EuFe_{2-x}Ru_xAs_2$ in the whole concentration range ($0 \leqslant x \leqslant 2$) is reported. Systematic electron spin resonance investigations of the Korringa-type Eu spin relaxation in combination with the results of band-structure calculations and magnetic susceptibility measurements can provide a clear picture of how the density of states is reduced by substituting Fe with Ru in $EuFe_2As_2$. Moreover, the strength of the exchange coupling between the local Eu and the itinerant spin systems can be estimated consistently with the weak coupling expected for this class of layered compounds.

DOI: 10.1103/PhysRevB.90.205105 PACS number(s): 74.70.Xa, 75.30.Fv, 76.30.−v

I. INTRODUCTION

In recent years, iron-based pnictides attracted considerable attention after the discovery of superconductivity in $LaFeAsO_{1-x}F_x$ [1] and related compounds with superconducting transition temperatures up to $T_{sc} = 55$ K [2,3]. In these quasi-two-dimensional structures, the superconductivity emerges from the FeAs layers, where it is induced by appropriate electron or hole doping. The corresponding undoped mother compounds are antiferromagnetic bad metals. To study the interplay of iron magnetism and superconductivity, the ternary AFe_2As_2 "122' '-systems (with $A =$ Ba, Sr, Ca, Eu) [4], which crystallize in the tetragonal $ThCr_2Si_2$ structure, provide a rich playground: these compounds have a spin-density wave (SDW) ground state and can be driven into superconductivity by chemical substitution on each of the lattice sites, e.g., by K on the A site [5,6], or Co for Fe [7,8], or P for As [9,10]. One of the most exciting compounds in the "122' '-family is $EuFe_2As_2$ with the highest reported SDW transition temperature $T_{SDW} =$ 190 K among these iron arsenides [11–13].

In spite of the large magnetic moments of the Eu^{2+} ions (electronic configuration $4f^7$, ground state with spin $S = 7/2$, $L = 0$) their influence on the magnetic and transport properties of the FeAs layers turned out to be weak [14,15]. Only below $T_N = 19$ K do the Eu spins undergo antiferromagnetic order [11,12]. However, already external magnetic fields above 1 T align the Eu spins ferromagnetically [16], while the FeAs layers remain unaffected up to the highest applied fields of 55 T [17]. Hydrostatic pressure [18] or the substitution of, e.g., P on the As site [10] even induce superconductivity coexisting with Eu magnetism. In consequence, due to the rather weak exchange coupling between the FeAs layers and the Eu spins, electron spin resonance on Eu^{2+} is well suited to study the physics of iron pnictides without strongly disturbing the conduction electron system [19–23]. A comprehensive overview on previous achievements of Eu-electron spin resonance (ESR) in iron pnictides can be found in Ref. [22]. Basically, at temperatures above T_{SDW} the ESR linewidth increases due to the Korringa relaxation of the Eu^{2+} spins at the conduction electrons. Concomitantly, the g value exhibits a shift with respect to the value in the insulating compounds due to the polarization of the spins of the conduction electrons. Thus, both the linewidth and g value locally probe the susceptibility of the conducting FeAs layers. In contrast, at temperatures below T_{SDW}, the Korringa relaxation is replaced by a line broadening via dipolar and ligand fields, as is typical for an insulator, although the conductivity is even higher than above T_{SDW}. It has been concluded that the Eu spins probe a part of the Fermi surface where an an energy gap opens at the SDW transition [22]. Substantial information on the transition to superconductivity was obtained in the case of dilution on the Eu site either by K substitution in $Eu_{0.5}K_{0.5}Fe_2As_2$ [21] or simultaneous substitution by Sr and Co in $Eu_{0.22}Sr_{0.78}Fe_{1.72}Co_{0.28}As_2$ [22]. A decrease of the linewidth stronger than linear with decreasing temperature just below T_{sc} is observed in both cases, discarding an isotropic BCS gap, which should result in a coherence peak. Nevertheless, an indication for a coherence peak has been found in the case of P substitution on the As site, i.e., the details of the superconductivity transition strongly depend on the type of substitution. Here, we focus on the substitution of Ru on the Fe site. The present study is motivated by the fact that the related substitution series $SrFe_{2-x}Ru_xAs_2$ shows superconductivity for ($0.6 \leqslant x \leqslant 0.8$) [24], which is mostly driven by chemical pressure [25]. Currently, anisotropic superconductivity has been observed in $EuFe_{1.50}Ru_{0.50}As_2$ [26]. In the following we discuss the local electronic properties (the density of states, DOS) of $EuFe_{2-x}Ru_xAs_2$ throughout the entire series ($0 \leqslant x \leqslant 2$) from the viewpoint of ESR, supported by resistivity and susceptibility measurements as well as density-functional band-structure calculations.

II. EXPERIMENTAL DETAILS

Polycrystalline samples of $EuFe_{2-x}Ru_xAs_2$ ($0 \leqslant x \leqslant 2$) were prepared by powder metallurgical techniques. Blended and compacted mixtures of precursor alloys EuAs, Fe_2As together with Ru and As powder were placed in glassy-carbon crucibles, welded into tantalum containers, and sealed into evacuated quartz tubes for heat treatment at 900°C for 24 h to 7 days followed by several grinding and densification steps. Samples were obtained in the form of sintered pellets. The sample quality has been confirmed by means of x-ray

 ©2014 American Physical Society

diffraction (XRD) analysis and electron-probe microanalysis (EPMA). For details see Refs. [8] and [25].

Magnetization (M) measurements have been performed using a commercial magnetometer (Quantum Design MPMS) at temperatures $2 \leqslant T \leqslant 400$ K and in external magnetic fields of 100 Oe, 1 kOe, and 10 kOe. The resistivity was measured on polycrystalline samples for $2 \leqslant T \leqslant 300$ K in zero magnetic field using the AC-transport option of a measurement system (Quantum Design PPMS) and utilizing the van der Pauw method [27]. The applied current had an amplitude of 10 mA and a frequency of 1.7 Hz.

ESR measurements were performed in a continuous wave spectrometer (Bruker) at X- and Q-band frequency ($\nu \approx 9.36$ and 34 GHz, respectively) in the temperature region $4.2 < T < 300$ K using a continuous He gas-flow cryostat (Oxford Instruments). ESR detects the power P absorbed by the sample from the transverse magnetic microwave field as a function of the static magnetic field H. The signal-to-noise ratio of the spectra is improved by recording the derivative dP/dH using a lock-in technique with field modulation.

Band-structure calculations were performed within the local-density approximation (LDA) using the full potential local orbital code FPLO [28] (version 9.01-35) with a k mesh of $24 \times 24 \times 24$ k points and the Perdew-Wang [29] parametrization of the exchange-correlation potential.

III. EXPERIMENTAL RESULTS

For all samples the crystal structure of $ThCr_2Si_2$ type (space group $I4/mmm$) was refined from powder XRD data by full-profile methods [Eu in $2a$ (0,0,0); Fe/Ru in $4d$ (0, 1/2, 1/4), and As in $4e$ (0, 0, z)]. The refined lattice parameters (Table I), the refined Ru occupancies, as well as EPMA unambiguously document the substitution of Fe by Ru. The nominal Ru contents are in good agreement with both the Ru occupancies from XRD and the EPMA data. As shown in Fig. 1, upon exchange of Fe by Ru a strong linear decrease is observed in the c parameter of the unit cell ($\approx -12\%$ for $x = 2$) accompanied by a weaker increase ($\approx 5\%$) of the a parameter. Note that the resulting unit-cell volume $V = a^2c$ increases with increasing Ru content for $0 \leqslant x \leqslant 0.75$ by $\approx 1\%$, but remains practically constant for higher x. This indicates that the lattice parameters are influenced not only by the size of the substituted ions but by electronic effects as well. The z parameter of As changes slightly but not systematically with the increase of the Ru content. However, the substitution leads to a strong decrease in the c/a ratio, this way drastically reducing the As-As distance along the c axis. This indicates a strong strain deformation with respect to the crystal lattice of the ternary Fe mother compound and suggests a change of the two-dimensional character of $EuFe_2As_2$ to a more three-dimensional one of $EuRu_2As_2$.

TABLE I. Tetragonal lattice parameters a and c and refined fractional coordinate z of As for various Ru concentrations x of $EuFe_{2-x}Ru_xAs_2$. Data for $x = 0$ are taken from Ref. [30].

x	a (Å)	c (Å)	z
0.00	3.9161(2)	12.052(6)	0.3625
0.25	3.9411(1)	11.9849(2)	0.3624(2)
0.50	3.9716(2)	11.8452(3)	0.3630(2)
1.00	4.0404(2)	11.4652(4)	0.3620(2)
1.50	4.1223(3)	11.0030(1)	0.3626(3)
1.75	4.1485(2)	10.8645(3)	0.3643(2)
2.00	4.1724(3)	10.7777(2)	0.3627(2)

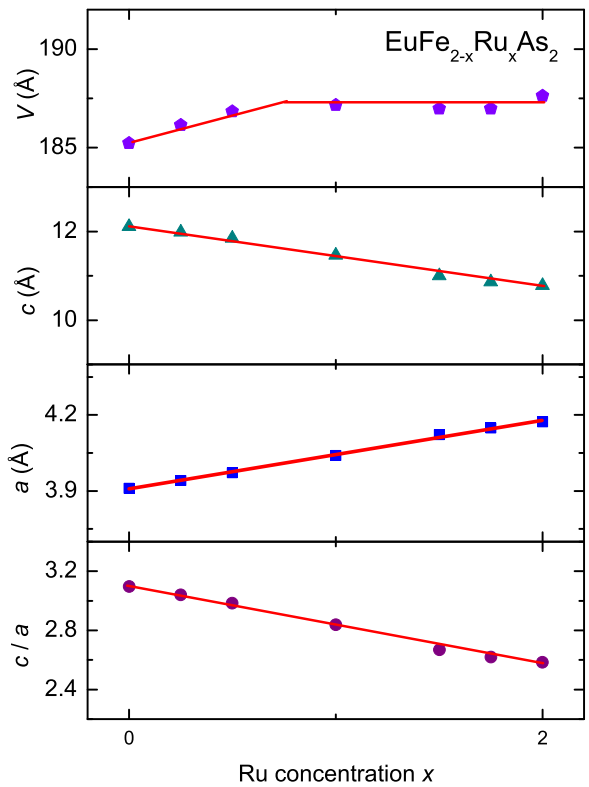

FIG. 1. (Color online) Tetragonal lattice parameters a, c, c/a and corresponding unit-cell volume V of $EuFe_{2-x}Ru_xAs_2$ in dependence of the ruthenium concentration x.

The temperature dependence of the normalized electrical resistivity is shown in Fig. 2. All compounds exhibit a linear increase of $\rho(T)$ as is typical for metals due to phonon scattering. The room temperature resistivity values are less than 1 mΩcm. Previous measurements in a series of $Eu(Fe_{1-x}Ru_x)_2As_2$ crystals revealed analogous results [31]. Because of the uncertainty of the absolute resistivity values due to grain boundaries in the polycrystalline samples, we prefer to plot the electrical resistivity normalized to its value at room temperature. The magnetic order of the Eu^{2+} spins causes a kink at T_C and a steeper decrease of $\rho(T)$ to lower temperatures. Superconductivity, indicated by zero resistivity, is observed for $x = 0.5$ at $T_{sc} = 23$ K, similar to the T_{sc} observed in the single crystal in Ref. [26]. The onset of superconductivity is partially inhibited and shifted to lower temperature due to the ferromagnetic order. Note also that the sample with $x = 0.25$ exhibits a broad hump close to the SDW transition at 125 K. Thus, $\rho(T)$ reveals an electronically driven phase transition in the substitution series.

The magnetic susceptibility $\chi = M/H$ of the $EuFe_{2-x}Ru_xAs_2$ samples is dominated by the Curie paramagnetic contribution of the localized Eu^{2+} moments

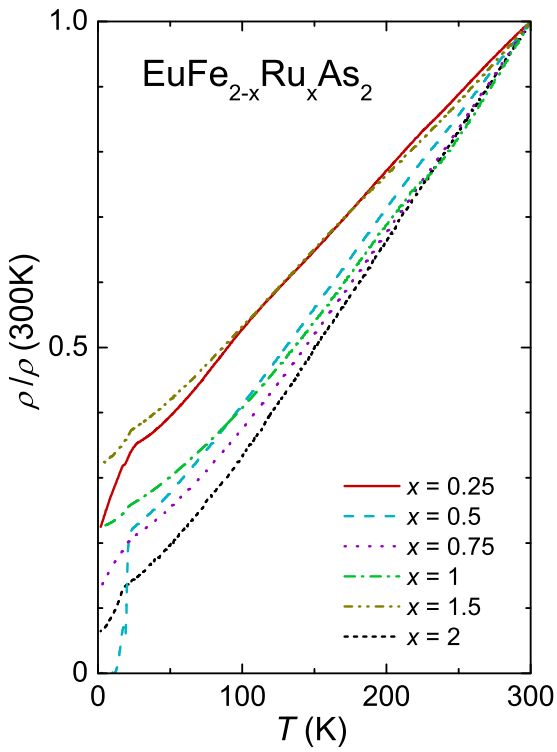

FIG. 2. (Color online) Temperature dependence of the resistivity $\rho(T)/\rho$ (300 K) (normalized at 300 K) for selected polycrystalline $EuFe_{2-x}Ru_xAs_2$ samples.

(spin $S = 7/2$). Plots of $\chi(T)$ measured in $H = 100$ Oe are presented for Fe-rich samples in Fig. 3 and for Ru-rich compositions in Fig. 4 (left panels). The onset of ferromagnetic order of the Eu^{2+} spins at $T_C \approx 20$ K varies only slightly with x. The value of T_C corresponding to the deflection points in the low-field magnetic susceptibility curves are given in the figures.

In some samples of iron-arsenide materials magnetization measurements indicated the presence of ferromagnetic impurity phases with $T_C > 400$ K, with a volume well below the resolution limit of XRD [8]. To saturate the magnetization of possible traces of such impurities the paramagnetic susceptibility of the $EuFe_{2-x}Ru_xAs_2$ samples was analyzed on data taken at $H = 10$ kOe (Figs. 3 and 4, right panels). The $1/\chi$ vs.

TABLE II. Fit parameters of the evaluation of the paramagnetic susceptibility and ordered magnetic moment at $T = 2$ K (see text). The values for $x = 2$ are in an excellent agreement with those obtained in Ref. [26]. Values for $x = 0$ and $x = 2$ are not included in Figs. 3 and 4.

x	μ_{eff} (μ_B)	Θ_{CW} (K)	χ_0 (10^{-3}emu mol^{-1})	m_{ord} (μ_B)
0.00	8.08	+19.0	+1.47	6.99
0.25	7.86	+22.6	+2.09	6.88
0.50	7.89	+23.1	+1.00	6.90
0.75	7.84	+23.5	+0.50	6.87
1.00	7.84	+23.7	+0.30	6.82
1.50	7.92	+24.3	+0.02	6.86
1.75	7.82	+22.7	−0.19	6.76
2.00	7.86	−19.8	−0.24	6.76

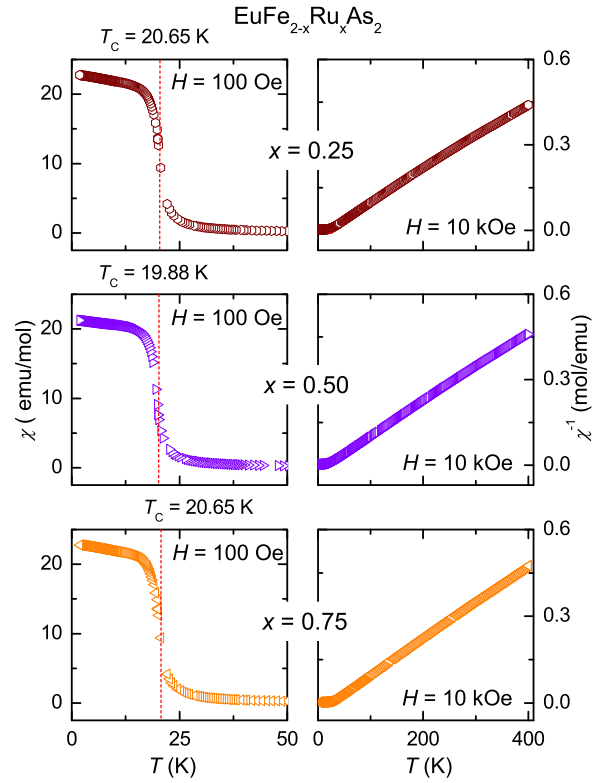

FIG. 3. (Color online) Temperature dependence of the magnetic susceptibility χ (left, $H = 100$ Oe) and its inverse $1/\chi$ (right, $H = 10$ kOe) for Fe-rich $EuFe_{2-x}Ru_xAs_2$ ($x < 1$). Dotted (red) lines indicate the magnetic transition temperatures.

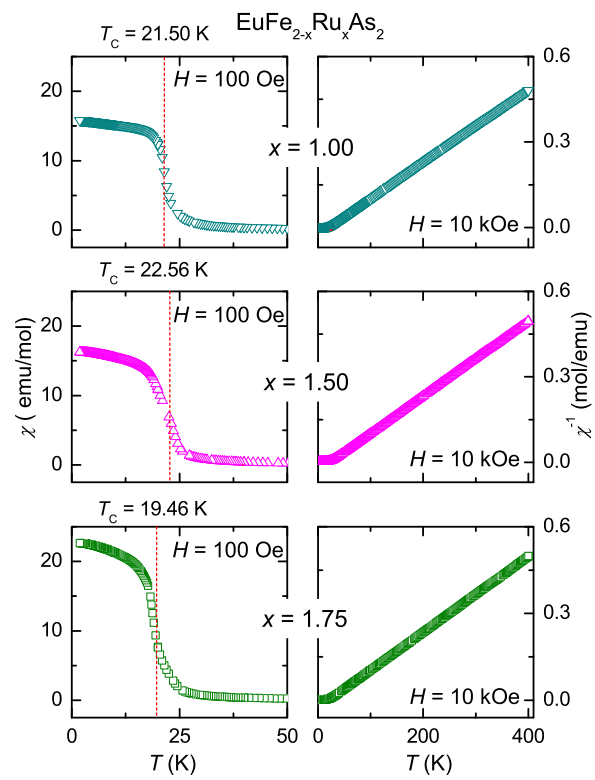

FIG. 4. (Color online) Temperature dependence of the magnetic susceptibility χ (left, $H = 100$ Oe) and its inverse $1/\chi$ (right, $H = 10$ kOe) for Ru-rich $EuFe_{2-x}Ru_xAs_2$ ($x \geqslant 1$).

T plots of samples with $x \leqslant 0.75$ are, however, still slightly curved downwards at high temperatures. Therefore, $\chi(T)$ was analyzed by a modified Curie-Weiss fit ($60 < T < 400$ K) including a temperature-independent term χ_0. All parameters of these fits as well as the ordered ferromagnetic moment are listed in Table II.

The effective moments μ_{eff} per formula unit turn out to be only slightly less than the theoretical value of a free Eu^{2+} ion of $7.94\mu_B$, indicating stable divalent Eu^{2+} ions. Also, the Curie-Weiss temperatures Θ_{CW} are always close to the values of the actual T_C. The ordered moments at 2 K (i.e., at about one tenth of T_C) in a field of 10 kOe are only a little below $7\mu_B$ and show almost no variation with the Ru content. Interestingly, a paramagnetic temperature-independent term χ_0 is observed for Fe-rich samples $x \leqslant 0.50$. This term decreases with x and gets obviously compensated by diamagnetic contributions for higher x (Table II). As can be taken from the strong field dependence of χ_0 for the $x = 0.25$ and $x = 0.50$ samples, (3.89×10^{-3} emu/mol and 3.05×10^{-3} emu/mol at $H =$ 100 Oe, respectively), a large part of this term is due to traces of the aforementioned impurities. The estimated mass fraction of the aforementioned ferromagnetic impurities is well below 0.1%. Therefore, with the large magnetic moment of Eu^{2+} and the presence of traces of ferromagnetic impurities, a meaningful interpretation of the development of χ_0 is ambigous.

However, the slow continuous decrease of χ_0 observed for samples with $x > 0.5$ might still be connected to a decrease of the Pauli paramagnetic susceptibility χ_P. A clearer picture of the development of the electronic DOS in an intermetallic alloy series is usually obtained from the analysis of the electronic specific heat (Sommerfeld coefficient γ). For the $EuFe_{2-x}Ru_xAs_2$ series such an analysis is also not feasible (due to the large contributions of the Eu^{2+} magnetic ordering to the specific heat at low temperatures). For these reasons, only a microscopic probe will provide reliable and accurate information on the development of the electronic DOS.

Figure 5 shows ESR spectra of $EuFe_{2-x}Ru_xAs_2$ with different Ru content x in the paramagnetic regime at $T =$ 35 K. Like in $EuFe_2As_2$ [19], all spectra consist of a single exchange-narrowed resonance which is well described by an asymmetrical Lorentz line. This is due to the skin effect, which appears in conductive compounds because of the interaction between the applied microwave field and mobile charge carriers. It yields an admixture of dispersion χ' to the absorption χ'' depending on the ratio of skin depth and sample size [32]. Because of the large linewidth ΔH, which is of comparable order of magnitude with the resonance field

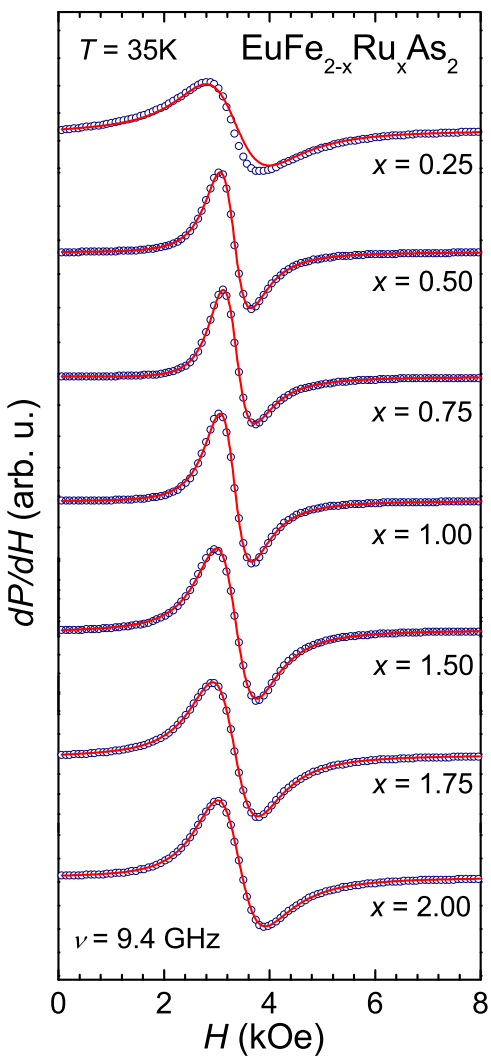

FIG. 5. (Color online) Typical ESR spectra of $EuFe_{2-x}Ru_xAs_2$ as obtained at $T = 35$ K. Solid (red) lines indicate a fit with asymmetrical Lorentz shape.

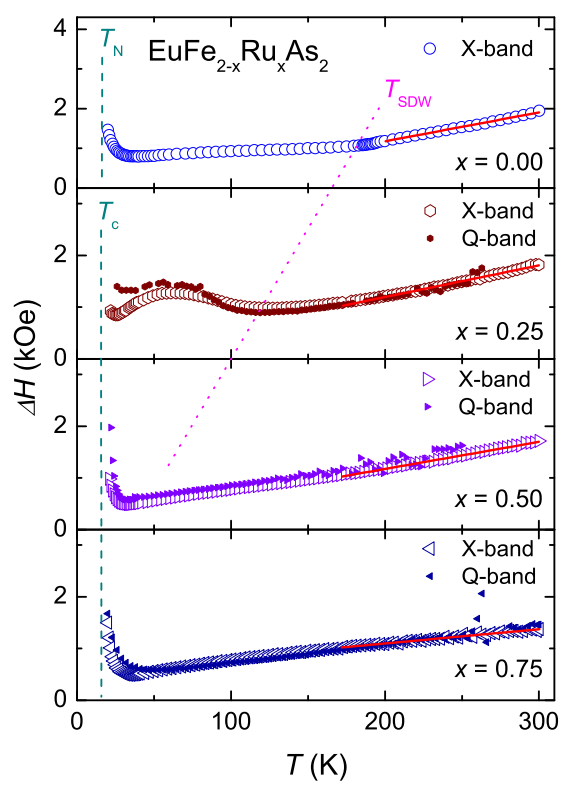

FIG. 6. (Color online) Temperature dependence of the ESR linewidth ΔH for Fe-rich $EuFe_{2-x}Ru_xAs_2$ ($x < 1$) measured at 9.4 and 36 GHz. The (red) solid lines represent the linear Korringa law. The X-band data of pure $EuFe_2As_2$ are taken from Ref. [19].

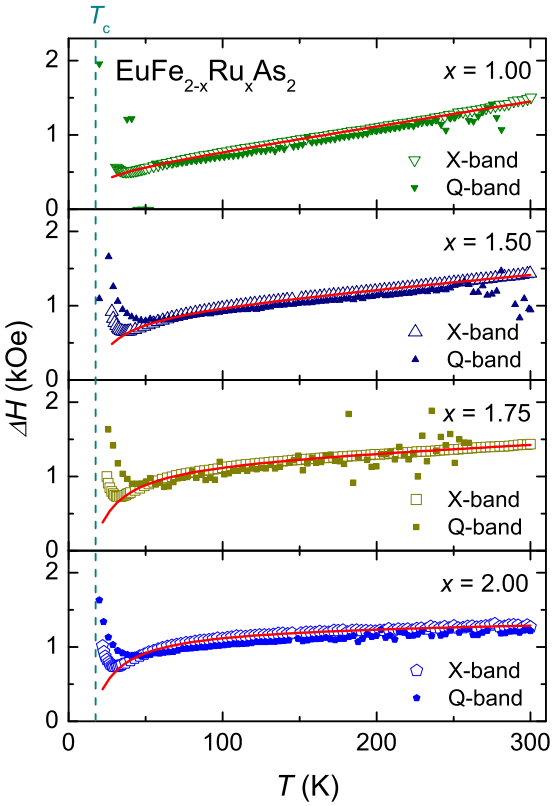

FIG. 7. (Color online) Temperature dependence of the ESR linewidth ΔH for Ru-rich $EuFe_{2-x}Ru_xAs_2$ ($x \geqslant 1$) measured at 9.4 and 36 GHz. The (red) solid lines represent a combined formula of Huber and Korringa laws.

H_{res}, the counterresonance at $-H_{res}$ had to be included in the fit as well [33].

For all samples the resonance field is approximately constant, close to $g = 2$ at high temperature, but shifts to lower fields on approaching magnetic order due to the local ferromagnetic polarization. At high temperatures the observed small deviations (≈3%) from the insulator value $g = 1.993$ of Eu^{2+} cannot be systematically evaluated due to the uncertainty in the asymmetry of the spectra, which in the case of the present broad lines strongly influences the fit value of the resonance field.

The most important information is obtained from the temperature dependence of the linewidth (Figs. 6 and 7). For completeness we added the data of pure $EuFe_2As_2$ taken from Ref. [19]. Up to $x = 0.25$ one clearly recognizes the SDW transition at T_{SDW}, which separates the usual metallic linear Korringa-relaxation regime at high temperatures from the saturating insulator-like relaxation regime at low temperatures. Moreover, the linewidth strongly increases upon approaching T_C from above because of critical magnetic fluctuations close to the phase transition. For $x \geqslant 0.5$, the linewidth increases approximately linearly with temperature indicating the dominant role of the Korringa relaxation of the localized Eu^{2+} spins via scattering of the conduction electrons [32]

$$\Delta H = bT = \frac{\pi k_B}{g\mu_B}\langle J^2(q)\rangle D^2(E_F)T, \qquad (1)$$

TABLE III. Fit parameters b, ΔH_∞, and $\sqrt{\langle J^2(q)\rangle}$ resulting from the evaluation of the temperature dependance of the ESR linewidth by Eqs. (1) and (2). The parameters for $x = 0$ are taken from Ref. [19]. Values of $\sqrt{\langle J^2(q)\rangle}$ are estimated via the relation between b and $D^2(E_F)$ given in Eq. (1). ΔH_0 is given only for distinct metallic behavior ($x < 1$).

x	b (Oe K^{-1})	ΔH_∞ (Oe)	$\sqrt{\langle J^2(q)\rangle}$ (meV)	ΔH_0 (Oe)
0.00	8	–	3.28	−456
0.25	6.2	–	3.17	−49
0.50	4.63	–	3.02	277
0.75	2.90	–	2.93	510
1.00	3.41	449	4.03	–
1.50	1.86	900	4.24	–
1.75	0.96	1198	3.33	–
2.00	0.30	1261	2.07	–

where $\langle J^2(q)\rangle$ denotes the squared exchange constant between localized spins and conduction electrons averaged over the momentum transfer q. $D(E_F)$ is the conduction-electron density of states (DOS) at the Fermi energy E_F, μ_B the Bohr magneton, and k_B the Boltzmann constant.

Comparing the behavior of the linewidth at high temperatures, one clearly recognizes a significant decrease of the Korringa slope b with increasing Ru content x. For the pure Ru compound the linewidth even seems to saturate at an asymptotic value, as is typical for an insulator rather than for a metal. As outlined by Huber *et al.* [34]

$$\Delta H = \frac{T - \Theta_{CW}}{T}\Delta H_\infty, \qquad (2)$$

where ΔH_∞ is the high-temperature value of the exchange-narrowed linewidth due to dipolar interactions between the Eu-spins and the zero-field splitting caused by the ligand field as described in Ref. [19]. Θ_{CW} is obtained from the static susceptibility measurements (cf. Table II). Thus for $x \geqslant 1.0$ we fitted the T dependence of ΔH by the sum of Eqs. (1) and (2) to separate insulator and metallic contributions. For x less than 1.0, we just added a constant residual linewidth ΔH_0 to Eq. (1) as is usually done in conventional metals. ΔH_0 represents the intercept of the linear Korringa law with the ordinate at $T = 0$. The results are given in Table III.

Finally, it is important to note that the data obtained at 34 GHz perfectly match those at 9.34 GHz. Therefore, a bottleneck scenario as suggested for powder samples of the Co-substituted $EuFe_2As_2$ [23] is not appropriate for Ru-substituted $EuFe_2As_2$ and hence, the spin-relaxation should give direct information on the DOS at the Fermi level. We also note that Rosa *et al.* observed an absence of Korringa behavior for $T > 100$ K in antiferromagnetic $EuIn_2As_2$ [35]. This provides a clear confirmation that the line broadening in the FeAs-based compounds is mainly driven by the relaxation of Eu^{2+} spins via Fe 3*d* electrons.

IV. THEORETICAL ANALYSIS AND DISCUSSION

For a deeper analysis of the Korringa relaxation we performed band-structure calculations to determine the DOS at the Fermi energy and to estimate the exchange coupling

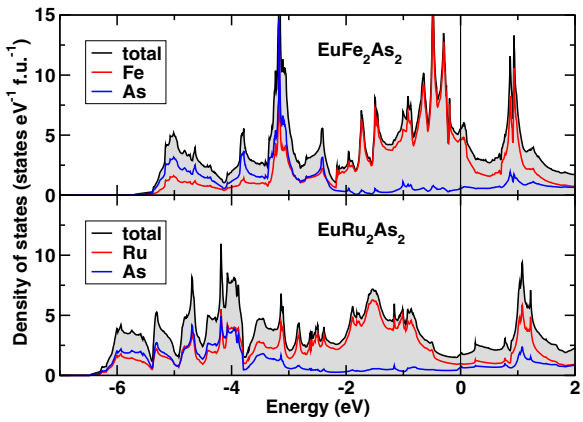

FIG. 8. (Color online) Total and partial density of states (DOS) of $EuFe_2As_2$ (upper panel) and $EuRu_2As_2$ (lower panel). The Fermi level E_F is at zero energy.

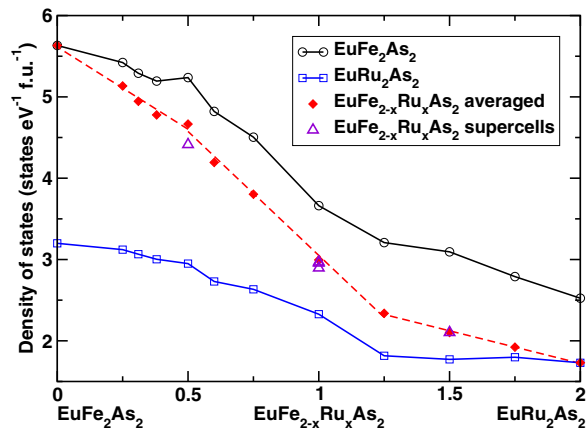

FIG. 9. (Color online) Total density of states (DOS) at the Fermi level for the $EuFe_{2-x}Ru_xAs_2$ substitution series. Symbols mark the actual calculated concentrations, lines are guides to the eye only. The (red) dashed lines are linear regressions for the x intervals [0.0,0.5], [0.5,1.25], [1.25,2.0].

strength between the Eu^{2+} ions and the conduction electrons. Such an itinerant description worked surprisingly well in $Ba_{1-x}K_x(Fe_{1-y}Co_y)_2As_2$ as described currently [36]. In the present case the main differences in the electronic DOS $D(E)$ of the valence bands for the mother compounds $EuFe_2As_2$ and $EuRu_2As_2$, as depicted in Fig. 8, are the (i) overall band width W and (ii) the ratio of the partial contributions originating from the transition metal and from As.

(i) The Fe compound has a considerably narrower band width by ~1 eV compared to the Ru system. This is related to the stronger covalence of the latter due to the spatially extended Ru 4d orbitals in contrast to the more localized Fe-3d states. In consequence, $D(E)$ of $EuFe_2As_2$ is in general higher than in $EuRu_2As_2$ since both compounds are (at least formally) isovalent and therefore the occupied $D(E)$ should scale with $1/W$.

(ii) In particular, the band narrowing caused by the smaller Fe-As hybridization affects the region in vicinity to the Fermi level: the bottom of the Fe-dominated part of $D(E)$ is at about -2 eV, whereas the Ru-dominated states extend down to about -4 eV. The stronger Ru-As hybridization is also obvious from the low-lying part of the valence band: whereas Ru and As contribute almost equally, this part is dominated by As states in $EuFe_2As_2$. In addition, the center of the occupied Ru states is by about 1-eV lower in binding energy than the respective Fe states. As a result, the combination of the features (i) and (ii) causes a strong reduction of $D(E_F)$ in the Ru system.

To separate the influence of the structural changes with increasing Ru substitution (lattice parameters and transition metal-As distances; see Fig. 9) from the changes caused by different electronic states of the substituent, we performed two types of calculations.

(1) Calculations for the two end-member compounds ($x = 0$ and $x = 2$), but considering the experimentally observed change of structural parameters within the full substitution series. In Fig. 9, the (black) circles ($x = 0$; $EuFe_2As_2$) and the (blue) squares ($x = 2$; $EuRu_2As_2$) are the average of two different models (LDA + U, open core treatment) for the strong correlations in the Eu-4f shell (the variance of the two models is rather small). To include a nominal Ru-substitution level into the modeling, the weighted average of these two curves according to the respective real composition was calculated, shown by the filled (red) diamonds.

(2) Supercell calculations were carried out for $x = 0.5$, $x = 1$, and $x = 1.5$. The results are marked by (purple) triangles and agree remarkably well with the simplified modeling 1 presented above, verifying this approach 1 *a posteriori*. To investigate the role of a specific Fe-Ru disorder, three different supercells have been constructed for $x = 1$. The resulting $D(E_F)$ values are basically identical [see Fig. 9, (purple) triangles at $x = 1$].

To study the influence of the structural changes, in particular the decreasing c axis and the related As-As distance, on the general topology of the Fermi surface, we also calculated the averaged Fermi velocity depending on the Ru content x. The pronounced two-dimensional character of the compound gets lost rather rapidly; for $x = 1$ we find already almost isotropic behavior comparing the Fermi velocities in and perpendicular to the tetragonal plane. The situation is very similar to the change of the electronic structure for $x = 0$, where the application of hydrostatic pressure [25] leads to a three-dimensional reconstruction of the two-dimensional Fermi surface at ambient pressure (cf. Fig. 6 in Ref. [25]).

In conclusion, we can attribute the strong decrease in the electronic density of states $D(E_F)$ in $EuFe_{2-x}Ru_xAs_2$ upon Ru substitution equally to structural effects as well as to a direct change in the transition-metal states. Also, a pronounced change in the slope of the $D(E)$ vs. concentration curve [(red) dashed lines] at $x \approx 0.5$ and $x \approx 1.5$ is observed. As finally shown in Fig. 10, the $D(E_F)$ obtained from our calculations can be directly related to the square root of the Korringa slope b measured by ESR. The data sets have been scaled in such a way that they coincide for $x = 0$. Note that both ordinates start from zero and that there is no additional residual contribution. The overall agreement of both data sets is reasonable and corroborates the simple Korringa relaxation as the dominant broadening mechanism giving direct access to the electronic DOS at the Fermi level. Moreover, using the theoretically derived $D(E_F)$ we can estimate the exchange

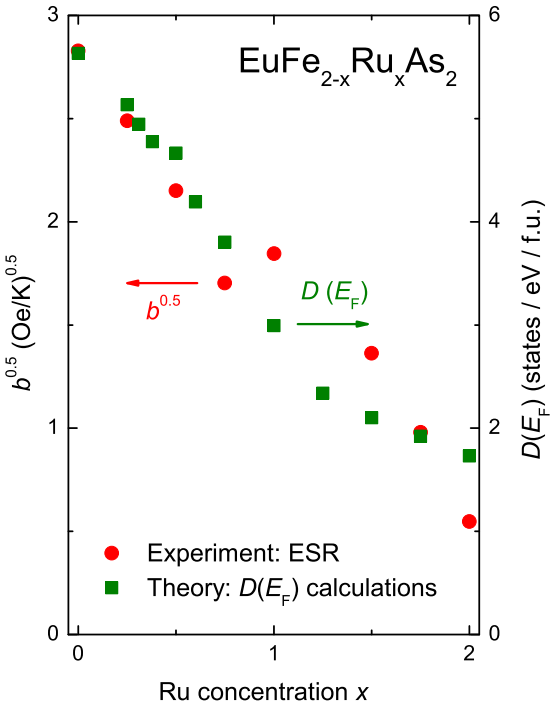

FIG. 10. (Color online) Comparison between Korringa slope and $D(E)$ at the Fermi level. The theoretical data set in Fig. 9 is the weighted average according to the Ru content x.

coupling $\sqrt{\langle J^2(q)\rangle}$ from the Korringa slope. The estimated values of $\sqrt{\langle J^2(q)\rangle}$ are in the order of several meV (Table III), which are in reasonable agreement with the values of Θ_{CW} given in Table II and comparable to the exchange values of 1–2 meV determined recently for $Ba_{1-x}Eu_xFe_2As_2$ [37]. In that analysis, the effects of electron-electron interactions have been included using specific heat and Pauli susceptibility to estimate the corresponding Stoner factor, which enhances the Korringa relaxation. Taking into account the Sommerfeld coefficient (γ) and the Pauli susceptibility (χ_P) of the reference compound $SrFe_{2-x}Ru_xAs_2$ [24], it turns out that in our case χ_P is not significantly enhanced with respect to γ. Therefore, we could neglect the Korringa exchange enhancement factor in our estimation.

V. SUMMARY

Electron spin resonance of Eu^{2+} ($4f^7$, $S = 7/2$) in europium-based iron pnictides successfully probes the local density of states of the conduction electrons. Starting from the mother compound $EuFe_2As_2$, the usual metallic phase is characterized by the linear increase of the linewidth on increasing temperature (Korringa slope $b = 8$ Oe K^{-1}) due to the Korringa relaxation via the conduction electrons, while this relaxation contribution is switched off in the spin-density wave phase ($T < T_{SDW}$), where the linewidth is mainly determined by the crystal-electric field of the ligands. Thus, we observe the same phenomenology like in insulators, in spite of the high conductivity. Substitution of ruthenium for iron gradually suppresses the SDW phase up to $x = 0.5$ and reduces the Korringa slope down to about $b = 0.3$ Oe K^{-1} for $x = 2$. This indicates a continuously decreasing conduction-electron density of states at the Fermi energy on increasing Ru substitution. The good agreement with band-structure calculations proves ESR to be the method of choice to access the density of states at the Fermi level in $EuFe_{2-x}Ru_xAs_2$, which allows, moreover, reliable estimations of the exchange coupling between the local and itinerant spin systems.

ACKNOWLEDGMENTS

We are very grateful to Dana Vieweg for susceptibility measurements and to Sebastian Widmann and Dieter Ehlers for technical support and discussion. This work has been supported by the German Research Foundation (DFG) via TRR 80 (Augsburg, München, Stuttgart), as well as by the DFG within the priority program SPP1458. M. Hemmida gratefully acknowledges the financial support from MPI-CPfS.

[1] Y. Kamihara, T. Watanabe, M. Hirano, and H. Hosono, J. Am. Chem. Soc. **130**, 3296 (2008).
[2] X. H. Chen, T. Wu, G. Wu, R. H. Liu, H. Chen, and D. F. Fang, Nature (London) **453**, 761 (2008).
[3] Z.-A. Ren, W. Lu, J. Yang, W. Yi, X.-L. Shen, Zheng-Cai, Guang-Can Che, X.-L. Dong, L.-L. Sun, F. Zhou, and Z.-X. Zhao, Chin. Phys. Lett. **25**, 2215 (2008).
[4] D. Kasinathan, A. Ormeci, K. Koch, U. Burkhardt, W. Schnelle, A. Leithe-Jasper, and H. Rosner, New J. Phys. **11**, 025023 (2009).
[5] M. Rotter, M. Tegel, and D. Johrendt, Phys. Rev. Lett. **101**, 107006 (2008).
[6] H. S. Jeevan, Z. Hossain, D. Kasinathan, H. Rosner, C. Geibel, and P. Gegenwart, Phys. Rev. B **78**, 092406 (2008).
[7] A. S. Sefat, R. Jin, M. A. McGuire, B. C. Sales, D. J. Singh, and D. Mandrus, Phys. Rev. Lett. **101**, 117004 (2008).
[8] A. Leithe-Jasper, W. Schnelle, C. Geibel, and H. Rosner, Phys. Rev. Lett. **101**, 207004 (2008).
[9] Z. Ren, Q. Tao, S. Jiang, C. Feng, C. Wang, J. Dai, G. Cao, and Z. Xu, Phys. Rev. Lett. **102**, 137002 (2009).
[10] H. S. Jeevan, D. Kasinathan, H. Rosner, and P. Gegenwart, Phys. Rev. B **83**, 054511 (2011).
[11] H. Raffius, M. Mörsen, B. D. Mosel, W. Müller-Warmuth, W. Jeitschko, L. Terbüchte, and T. Vomhof, J. Phys. Chem. Solids **54**, 135 (1993).
[12] H. S. Jeevan, Z. Hossain, D. Kasinathan, H. Rosner, C. Geibel, and P. Gegenwart, Phys. Rev. B **78**, 052502 (2008).
[13] D. Wu, N. Barisic, N. Drichko, S. Kaiser, A. Faridian, M. Dressel, S. Jiang, Z. Ren, L. J. Li, G. H. Cao, Z. A. Xu, H. S. Jeevan, and P. Gegenwart, Phys. Rev. B **79**, 155103 (2009).
[14] B. Zhou, Y. Zhang, L.-X. Yang, M. Xu, C. He, F. Chen, J.-F. Zhao, H.-W. Ou, J. Wei, B.-P. Xie, T. Wu, G. Wu, M. Arita, K. Shimada, H. Namatame, M. Taniguchi, X. H. Chen, and D. L. Feng, Phys. Rev. B **81**, 155124 (2010).

[15] T. Terashima, N. Kurita, A. Kikkawa, H. S. Suzuki, T. Matsumoto, K. Murata, and S. Uji, J. Phys. Soc. Jpn. **79**, 103706 (2010).
[16] S. Jiang, Y. Luo, Z. Ren, Z. Zhu, C. Wang, X. Xu, Q. Tao, G. Cao, and Z. Xu, New J. Phys. **11**, 025007 (2009).
[17] M. Tokunaga, I. Katakura, N. Katayama, and K. Ohgushi, J. Low Temp. Phys. **159**, 601 (2010).
[18] N. Kurita, M. Kimata, K. Kodama, A. Harada, M. Tomita, H. S. Suzuki, T. Matsumoto, K. Murata, S. Uji, and T. Terashima, Phys. Rev. B **83**, 100501(R) (2011).
[19] E. Dengler, J. Deisenhofer, H.-A. Krug von Nidda, Seunghyun Khim, J. S. Kim, Kee Hoon Kim, F. Casper, C. Felser, and A. Loidl, Phys. Rev. B **81**, 024406 (2010).
[20] J. J. Ying, T. Wu, Q. J. Zheng, Y. He, G. Wu, Q. J. Li, Y. J. Yan, Y. L. Xie, R. H. Liu, X. F. Wang, and X. H. Chen, Phys. Rev. B **81**, 052503 (2010).
[21] N. Pascher, J. Deisenhofer, H.-A. Krug von Nidda, M. Hemmida, H. S. Jeevan, P. Gegenwart, and A. Loidl, Phys. Rev. B **82**, 054525 (2010).
[22] H.-A. Krug von Nidda, S. Kraus, S. Schaile, E. Dengler, N. Pascher, M. Hemmida, M. J. Eom, J. S. Kim, H. S. Jeevan, P. Gegenwart, J. Deisenhofer, and A. Loidl, Phys. Rev. B **86**, 094411 (2012).
[23] F. A. Garcia, A. Leithe-Jasper, W. Schnelle, M. Nicklas, H. Rosner, and J. Sichelschmidt, New J. Phys. **14**, 063005 (2012).
[24] W. Schnelle, A. Leithe-Jasper, R. Gumeniuk, U. Burkhardt, D. Kasinathan, and H. Rosner, Phys. Rev. B **79**, 214516 (2009).
[25] D. Kasinathan, M. Schmitt, K. Koepernik, A. Ormeci, K. Meier, U. Schwarz, M. Hanfland, C. Geibel, Y. Grin, A. Leithe-Jasper, and H. Rosner, Phys. Rev. B **84**, 054509 (2011).
[26] Wen-He Jiao, Qian Tao, Jin-Ke Bao, Yun-Lei Sun, Chun-Mu Feng, Zhu-An Xu, I. Nowik, I. Felner, and Guang-Han Cao, Europhys. Lett. **95**, 67007 (2011).
[27] L. J. van der Pauw, Philips Tech. Rev. **20**, 220 (1958).
[28] K. Koepernik and H. Eschrig, Phys. Rev. B **59**, 1743 (1999).
[29] J. P. Perdew and Y. Wang, Phys. Rev. B **45**, 13244 (1992).
[30] W. Uhoya, G. Tsoi, Yogesh K. Vohra, M. A. McGuire, A. S. Sefat, B. C. Sales, D. Mandrus, and S. T. Weir, J. Phys.: Condens. Matter **22**, 292202 (2010).
[31] Wen-He Jiao, Qian Tao, Jin-Ke Bao, Hao Jiang, Chun-Mu Feng, Zhu-An Xu, and Guang-Han Cao, J. Phys.: Conf. Series **400**, 022038 (2012).
[32] S. E. Barnes, Adv. Phys. **30**, 801 (1981).
[33] J. P. Joshi and S. V. Bhat, J. Magn. Reson. **168**, 284 (2004).
[34] D. L. Huber, G. Alejandro, A. Caneiro, M. T. Causa, F. Prado, M. Tovar, and S. B. Oseroff, Phys. Rev. B **60**, 12155 (1999).
[35] P. F. S. Rosa, C. Adriano, T. M. Garitezi, R. A. Ribeiro, Z. Fisk, and P. G. Pagliuso, Phys. Rev. B **86**, 094408 (2012).
[36] T. Goltz, V. Zinth, D. Johrendt, H. Rosner, G. Pascua, H. Luetkens, P. Materne, and H.-H. Klauss, Phys. Rev. B **89**, 144511 (2014).
[37] P. F. S. Rosa, C. Adriano, W. Iwamoto, T. M. Garitezi, T. Grant, Z. Fisk, and P. G. Pagliuso, Phys. Rev. B **86**, 165131 (2012).